

Supplemental Information

Experimental Section:

Characterizations

XRD measurements were carried out using an automated Rigaku X-ray diffractometer with monochromatic Cu K α radiation. XPS measurements were performed at room temperature utilizing a Kratos AXIS Ultra Imaging XPS Spectrometer using a monochromated Al K α X-ray source operated at 150 W. The area of analysis was $\sim 700 \mu\text{m} \times 300 \mu\text{m}$. Survey spectra and high resolution elemental region spectra were acquired using analyzer pass energies of 160 and 20 eV respectively. FTIR spectra were obtained using a Perkin-Elmer Spectrum One Instrument in conjunction with a Golden Gate ATP setup utilizing a spectral resolution of 2 cm^{-1} . Micro-FTIR spectra of pre/post decomposition samples were recorded against pure samples in the range of 4000 to 600 cm^{-1} using a Nicolet iN10 MX FTIR Microscope.

Solid-state ^{11}B and ^{27}Al MAS NMR spectra were obtained on a Varian NMR spectrometer (400 MHz). The experiments were performed at ambient temperatures using air-tight end-capped zirconia rotors, which were packed with the sample in the glovebox and spun at 12–15 kHz. The spectral frequencies were 160.5 and 130.3 MHz for the ^{11}B and ^{27}Al nuclei, respectively. The ^{27}Al NMR chemical shift scale (ppm) was referenced externally with $[\text{Al}(\text{H}_2\text{O})_6]^{3+}$ in aqueous solution to 0 ppm while ^{11}B NMR were referenced to 0 ppm with $\text{BF}_3 \cdot \text{OEt}_2$.

TPD measurements were performed on a Quantachrome Autosorb IQ Cor100 using a heating rate of $5 \text{ }^\circ\text{C min}^{-1}$ and a carrier gas of argon at a flow rate of $60 \text{ mL} \cdot \text{min}^{-1}$. Isothermal desorption/absorption and quantification of hydrogen evolution were obtained with a Hy-Energy PCT Pro-2000 instrument. Both MS signals were recorded using a mass spectrometer PrismaPlus PFEIFFER QME220.

Elemental analysis of carbon, hydrogen, and nitrogen were performed using an Elementar Vario MICRO CUBE analyzer. Elemental analysis of aluminum and boron were performed using a Leeman PROFILE SPEC Inductively Coupled Plasma-Atomic Emission Spectrometer.

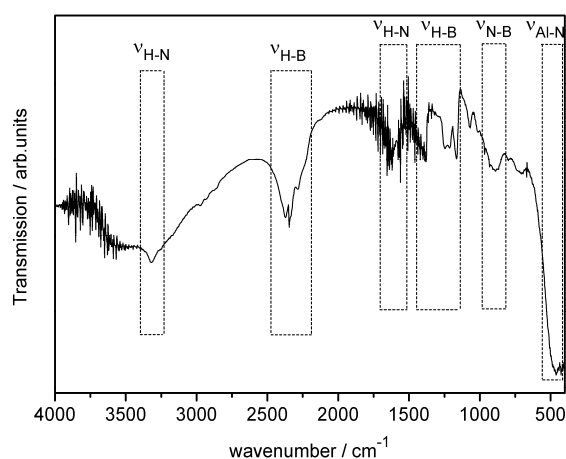


Figure S1. FTIR spectrum of as-prepared $\text{Al}(\text{NH}_2\text{BH}_3)_3 \cdot 3\text{NH}_3$.



Figure S2. Photograph of pressed shaped $\text{Al}(\text{NH}_2\text{BH}_3)_3 \cdot 3\text{NH}_3$ powder after exposure to dry air for 3 days.

Table S1. Experimentally measured vibrational modes of as-prepared $\text{Al}(\text{NH}_2\text{BH}_3)_3 \cdot 3\text{NH}_3$ (cm^{-1}). ^{[a][b]}

Molecule	Experimental	Theory [1,2]	Vibrational modes
$\text{NH}_3/\text{Al}(\text{NH}_3)_6^{3+}$	426	439	Al-N stretching
	1014, 1620	1027, 1620	H-N scissoring
	3319	3421	H-N symmetric stretching
	-	3540	H-N antisymmetric stretching
$\text{AlAB}/\text{Al}(\text{NH}_2\text{BH}_3)_6^{3-}$	461	-	H antisymmetric rocking with Al-N stretching/Al-N stretching
	726, 780, 798	-	antisymmetric H-N, H-B deformation/H wagging
	875	861	N-B stretching
	1066, 1112	987–1117	H wagging
	1165, 1248, 1380	1124–1211, 1380	H-B scissoring
	1555	1550	H-N scissoring
	2116	-	-
	2200, 2283	2178–2186	H-B symmetric stretching
	2341, 2372	2225–2309	H-B antisymmetric stretching
	3250	3335–3342	H-N symmetric stretching
-	3412–3415	H-N antisymmetric stretching	

^[a] “-” indicates that no relevant data are available; ^[b] Part of the theory data are based on DFT studies of LiAB and AlH_3NH_3 .

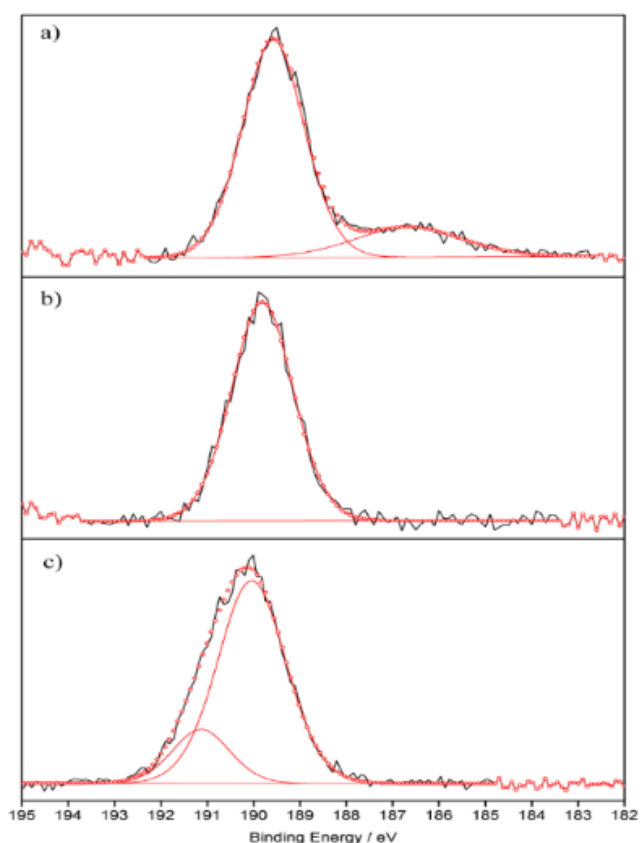


Figure S3. The B 1s XPS results of $\text{Al}(\text{NH}_2\text{BH}_3)_3 \cdot 3\text{NH}_3$ before (a) and after thermal decomposition in an open system (b)/in a closed system (c). The experiment data are in black, while the fitted ones are in red.

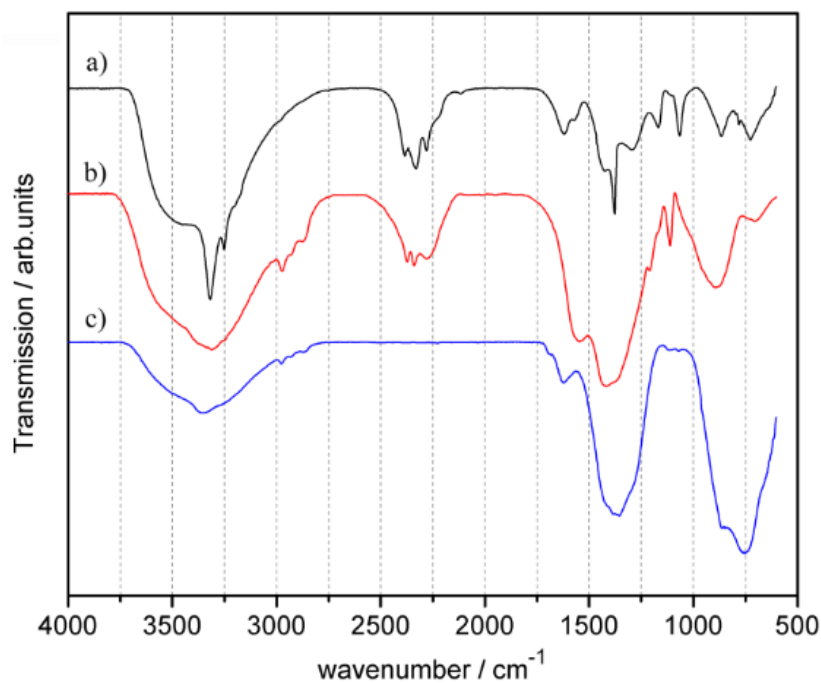


Figure S4. Micro-FTIR spectra: (a) $\text{Al}(\text{NH}_2\text{BH}_3)_3 \cdot 3\text{NH}_3$, (b) $\text{AlN}_3\text{B}_3\text{H}_6$, (c) $\text{AlN}_6\text{B}_3\text{H}_{6.5}^*$. $\text{AlN}_3\text{B}_3\text{H}_6$ (open system) and $\text{AlN}_6\text{B}_3\text{H}_{6.5}^*$ (closed system) are generated from $\text{Al}(\text{NH}_2\text{BH}_3)_3 \cdot 3\text{NH}_3$ decomposition.

Table S2. Experimentally measured vibrational modes of $\text{AlN}_3\text{B}_3\text{H}_6$ and $\text{AlN}_6\text{B}_3\text{H}_{6.5}^*$ (cm^{-1}).

Molecule	Experimental	Vibrational modes
$\text{AlN}_3\text{B}_3\text{H}_6$	706, 893	Al-N stretching/ AlN [3–5]
	1108	H wagging
	1170, 1207	H-B scissoring
	1390, 1544	N-B stretching/ h -BN [6,7]
	2283	H-B symmetric stretching
	2340, 2373	H-B antisymmetric stretching
	2877, 2929, 2969	H-N or H-O deformation
$\text{AlN}_6\text{B}_3\text{H}_{6.5}^*$	748, 858	Al-N stretching/ AlN [3–5]
	1068, 1114	H wagging
	1367, 1627	N-B stretching/ h -BN [6,7]
	2868, 2931, 2979	H-N or H-O deformation

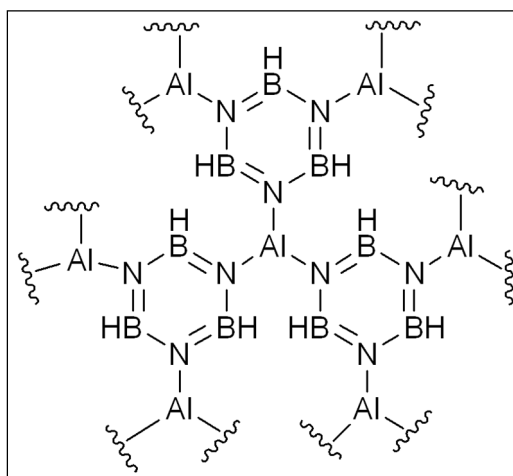
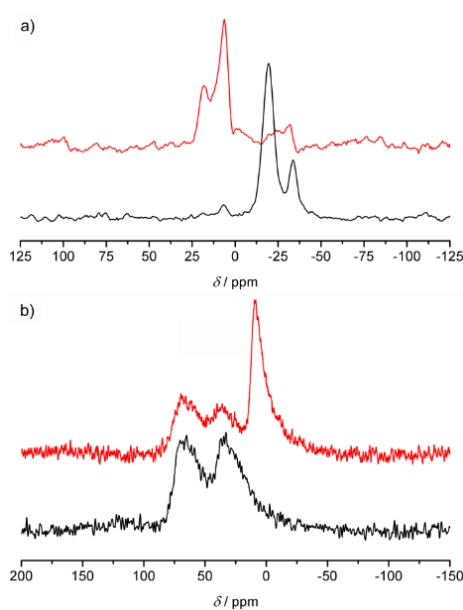
**Figure S5.** Structural representation borazine-derived $\text{AlN}_3\text{B}_3\text{H}_6$.**Figure S6.** (a) ^{11}B CPMAS NMR spectra and (b) ^{27}Al CPMAS NMR spectra of as-prepared (black) $\text{Al}(\text{NH}_2\text{BH}_3)_3 \cdot 3\text{NH}_3$ and after desorption at $105\text{ }^\circ\text{C}$ (red) in a closed vessel.

Table S3. Elemental analysis of $\text{Al}(\text{NH}_2\text{BH}_3)_3 \cdot 3\text{NH}_3$ before and after thermal decomposition in an open system/in a closed system (%).

Sample	Al	N	B	H	C
$\text{Al}(\text{NH}_2\text{BH}_3)_3 \cdot 3\text{NH}_3$	15.16	44.74	18.45	13.51	–
$\text{AlAB} \cdot 3\text{NH}_3$ decomposition open system	20.19	37.54	23.65	6.28	0.16
$\text{AlAB} \cdot 3\text{NH}_3$ decomposition closed system	15.83	48.18	18.36	3.83	0.13

References

1. Lee, S.M.; Kang, X.D.; Wang, P.; Cheng, H.M.; Lee, Y.H. A comparative study of the structural, electronic, and vibrational properties of NH_3BH_3 and LiNH_2BH_3 : Theory and experiment. *ChemPhysChem* **2009**, *10*, 1825–1833.
2. Leboeuf, M.; Russo, N.; Salahub, D.R.; Toscano, M. A density functional study of borane and alane monoammoniate ($\text{BH}_3\text{NH}_3, \text{AlH}_3\text{NH}_3$). *J. Chem. Phys.* **1995**, *103*, 7408–7413.
3. Danh, N.Q.; Monz, K.H.; Pulker, H.K. Reactive low voltage ion plating of aluminium nitride films and their characteristics. *Thin Solid Films* **1995**, *257*, 116–124.
4. Ying, J.Y. Processing of Nanocrystalline Nitrides and Oxide Composites. Available online: <http://oai.dtic.mil/oai/oai?verb=getRecord&metadataPrefix=html&identifier=ADA369525> (accessed on 6 July 2015).
5. Jiang, N.; Xu, S.; Ostrikov, K.N.; Chai, J.W.; Li, Y.N.; Ling, K.M.; Lee, S. Synthesis and structural properties of Al-C-N-O composite thin films. *Thin Solid Films* **2001**, *385*, 55–60.
6. Geick, R.; Perry, C.H.; Ruppert, G. Normal modes in hexagonal boron nitride. *Phys. Rev.* **1966**, *146*, 543–547.
7. Ohba, N.; Miwa, K.; Nagasako, N.; Fukumoto, A. First-principles study on structural, dielectric, and dynamical properties for three BN polytypes. *Phys. Rev. B* **2001**, *63*, 115207.